

Damage detection using piezoelectric transducers and the Lamb wave approach: II. Robust and quantitative decision making

Y Lu¹, X Wang¹, J Tang^{1,3} and Y Ding²

¹ Department of Mechanical Engineering, University of Connecticut, Storrs, CT 06269, USA

² Department of Industrial and Systems Engineering, Texas A&M University, College State, TX 77843, USA

E-mail: jtang@engr.uconn.edu

Received 6 November 2007, in final form 25 January 2008

Published 11 March 2008

Online at stacks.iop.org/SMS/17/025034

Abstract

The propagation of Lamb waves generated by piezoelectric transducers in a one-dimensional structure has been studied comprehensively in part I of this two-paper series. Using the information embedded in the propagating waveforms, we expect to make a decision on whether damage has occurred; however, environmental and operational variances inevitably complicate the problem. To better detect the damage under these variances, we present in this paper a robust and quantitative decision-making methodology involving advanced signal processing and statistical analysis. In order to statistically evaluate the features in Lamb wave propagation in the presence of noise, we collect multiple time series (baseline signals) from the undamaged beam. A combination of the improved adaptive harmonic wavelet transform (AHWT) and the principal component analysis (PCA) is performed on the baseline signals to highlight the critical features of Lamb wave propagation in the undamaged structure. The detection of damage is facilitated by comparing the features of the test signal collected from the test structure (damaged or undamaged) with the features of the baseline signals. In this process, we employ Hotelling's T^2 statistical analysis to first purify the baseline dataset and then to quantify the deviation of the test data vector from the baseline dataset. Through experimental and numerical studies, we systematically investigate the proposed methodology in terms of the detectability (capability of detecting damage), the sensitivity (with respect to damage severity and excitation frequency) and the robustness against noises. The parametric studies also validate, from the signal processing standpoint, the guidelines of Lamb-wave-based damage detection developed in part I.

1. Introduction

Structural damage detection using Lamb waves excited and sensed by embedded piezoelectric transducers has shown many promising features. Lamb waves, which are elastic guided waves propagating in a solid plate (or layer) with free boundaries, have been well studied and widely used in damage detection. In recent years, a significant amount of research on the modeling and analysis has been carried out

to further understand the properties of Lamb waves excited by piezoelectric transducers (Lin and Yuan 2001a, 2001b, Giurgiutiu 2005, Raghavan and Cesnik 2005). In general, Lamb waves are more sensitive to the presence of local damage than the global response of a structure; thus the Lamb wave techniques could provide more useful information than vibration-based techniques (Kessler and Dunn 2003) in certain cases. This promising advantage provides possibilities of *in situ* damage detection in various applications.

Based on the information given by the Lamb wave propagation, previous researchers have developed a variety

³ Author to whom any correspondence should be addressed.

of damage detection or identification schemes to determine the status of a structure. One straightforward thought is to compare the time domain signals collected from undamaged and damaged structures. To quantify the degree by which the signals differ from each other, a number of damage indices have been proposed (Tseng and Naidu 2002), e.g. root-mean-square deviation (RMSD), mean absolute percentage deviation (MAPD), covariance (Cov) and correlation coefficient (CC). Most of these indices are scalars which average the difference over the time period; thus some time information has to be sacrificed. To take advantage of both the amplitude and the time information, the use of time-of-flight (TOF) has been suggested, which measures the traveling time of a wavepacket from the actuator to the sensor. Some identification methodologies depend more or less on the time-of-flight concept. For example, Lin and Yuan (2001a, 2001b) presented a damage identification scheme using a migration technique which treats the damage as a secondary source and the detected reflection waves are back-propagated towards the damage. Giurgiutiu *et al* (2003) explored using the weighted sum of the wave propagation signals in different directions collected by a sensor array. However, since the signals are often contaminated with noise, in certain cases the time-of-flight may not be measured accurately enough to determine the damage location. Moreover, due to the complexity of multi-mode Lamb wave propagation, blind zones may exist, where extra caution and effort is needed (Tua *et al* 2004).

In many applications, the timely detection of the occurrence of damage is of primary concern, especially in the presence of environmental uncertainties which make the identification of damage location/severity difficult. The environmental and operational variances (e.g. ground vibration or electrical disturbances) result in noisy and complex sensor data. Since any 'robust' decision-making scheme requires proper handling of noise, the importance of signal processing has gradually been emphasized (Staszewski 2002). To reduce the noise effect, it is common to collect multiple signals from the same structure under the same conditions. One straightforward and widely used signal processing method is to directly average multiple signals (Raghavan and Cesnik 2005), but such a method does not take full usage of the information from the statistical point of view. Filtering techniques, e.g. the Chebyshev type II bandpass filter (Yu and Giurgiutiu 2005), are adopted by some researchers. Recently, denoising by using either the discrete (Yu and Giurgiutiu 2006) or the continuous wavelet transform (Yan *et al* 2005) has also been studied, which essentially leads to signal processing techniques in feature domains other than the usual time domain. Here arises the issue of feature extraction and representation. The Fourier transform, though most widely used (Cawley and Adams 1979, Doebling *et al* 1996), provides only the global frequency information over the entire time span but loses all the time information in the signal. To overcome this drawback, the short time Fourier transform (STFT) was developed to map a signal into a two-dimensional function of time and frequency (Niethammer 1999, Zhao *et al* 2006). STFT adopts a windowing technique, but the resolution depends on the size of the window, which is referred to as the uncertainty principle

(Papoulis 1962): a small window leads to fine time resolution but coarse frequency resolution, while a large window has the opposite effect. Wavelet analysis is another joint time–frequency domain technique, which can be treated as a short time Fourier transform with variable-sized windows. It is essentially a correlation-based method that yields coefficients representing how well the input signal correlates with a series of windowed functions which are the wavelet basis. Kim and Melhem (2004) reviewed recent studies on damage detection using wavelet analysis and put them into three categories: (1) variation of wavelet coefficients; (2) local perturbation of wavelet coefficients and (3) reflective wave caused by local damage. The detectability (capability of detecting damage) thus relies on the degree by which the waveform signal of a test structure differs from that of an undamaged structure. A variety of mother wavelets have been used, including Haar wavelets (Wang *et al* 1999), Daubechies wavelets (Hou *et al* 2000), Mexican hat wavelets (Lu and Hsu 1999), Gabor wavelets (Quek *et al* 2001), Morlet wavelets (Park *et al* 2006), etc.

Using wavelet analysis for feature extraction, we can transform each time series collected into one array of wavelet coefficients. In the presence of environmental and operational variances, multiple signals are collected from the undamaged structure; thus a matrix instead of only one vector of wavelet coefficients will be obtained as the baseline dataset. Although it is possible to use the aforementioned damage indices, the complexity due to multiple baseline signals may affect the accuracy or even the feasibility. Indeed, statistical techniques appear to be a natural choice. The research issue here is actually similar to that in process monitoring, where multivariate data are collected from different processes and used to determine abnormal operational conditions. Ganesan *et al* (2004) performed a thorough literature review on wavelet-based multiscale statistical techniques in the field of process monitoring, where it was pointed out that the principal component analysis (PCA) combined with Hotelling's T^2 analysis could be very useful for monitoring. PCA is an orthogonal linear transformation that projects data onto a new coordinate system such that the largest variance lies on the first coordinate (first principal component), the second greatest variance on the second coordinate, and so on. In some applications, the obtained wavelet features are compressed and denoised by the truncation of the principal components with the corresponding eigenvalues below a certain threshold (Okimoto and Lemonds 1999). The PCA is usually followed by a decision-making procedure based on Hotelling's T^2 , which is a statistic for a multivariate test of differences between the mean values of two data groups. In damage detection studies, the T^2 statistic not only can quantitatively detect a damage with a given confidence level, but also can help eliminate outliers from the set of baseline signals (Fang and Tang 2006).

2. Research overview

Although a significant amount of research has been carried out on Lamb-wave-based damage detection using piezoelectric transducers, there are still unsolved issues regarding detection

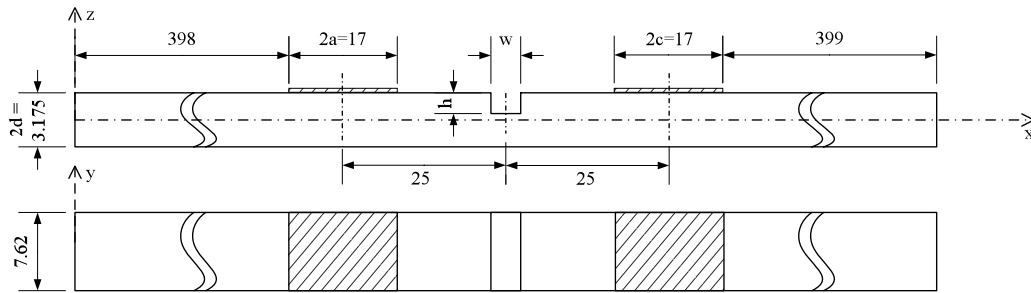


Figure 1. Side and top view of the experimental set-up (dimensions in mm).

decision-making algorithms. In particular, to date, the feature extraction and quantitative prediction of damage in the presence of environmental uncertainties remain as a challenging problem. Existing methods are either built upon the accurate analysis of wave propagation that might not be measured easily under noisy conditions, or using an overly simplified threshold value that is rigid and overlooks the abundant information carried by the wave propagation signals. In this research, a combination of signal analysis tools will be studied to specifically address the issue of robust damage detection using piezoelectric transducers and the Lamb wave propagation.

The damage detection is carried out by comparing the multiple time series (baseline signals) measured *a priori* from the undamaged structure with one test signal collected from the test beam (damaged or undamaged). In order to identify the critical features embedded in the baseline signals, we adopt the adaptive harmonic wavelet transform to analyze the wave propagation characteristics. This adaptive harmonic wavelet transform allows us to use the smallest number of wavelet coefficients (referred to as the baseline dataset) to characterize the multiple signals in the joint time–frequency domain. Following that, the principal component analysis is applied to the wavelet coefficients for feature highlighting and denoising. During the detection process, the test signal will undergo the same data processing; thus a vector of wavelet coefficients of the test signal (the test data vector) is obtained. Finally, we use Hotelling's T^2 analysis to analyze quantitatively the difference between the test data vector and the baseline dataset, where the decision making is made upon a given confidence level. With this highly integrated procedure, human interference can be reduced so that the damage detection may become an automated process. Using this quantitative and robust decision-making procedure, we then investigate the influence of a variety of system parameters involved in the Lamb-wave-based damage detection using piezoelectric transducers.

This paper is part II of a two-paper series. In part I, systematic analysis of Lamb wave propagation excited and sensed by piezoelectric transducers is performed. Parametric studies have verified the 'sweet spot' excitation center frequency concept that maximizes the amplitude ratio between the S_0 and A_0 mode waves. In this second paper, the parametric results obtained in part I will be examined in actual damage detection with environmental and operational variances. This

two-paper series will provide general guidelines for Lamb-wave-based damage detection using piezoelectric transducers.

3. Description of decision-making methodology

As mentioned above, for signals like Lamb waves that contain non-stationary content, time–frequency analysis is preferred rather than frequency-only methods (Peng and Chu 2004). Among various time–frequency representations, wavelet analysis has the ability of multiscale decomposition via dilation and translation; thus, features in a signal can be extracted through wavelet basis (Yu and Giurgiutiu 2005). The advantage of wavelet transforms is the flexibility in using narrow windows for the analysis of high frequency content and wide windows for low frequencies. Newland (1993, 1994) developed the harmonic wavelet and its generalized form, whose wavelet levels represent non-overlapping frequency bands so that there is no interference term between any frequency components. It is preferable if the information contained in the original signals can be isolated and concentrated in the wavelet domain, so that the decision about damage status could be made based on as few coefficients (i.e. features) as possible. Newland's harmonic wavelet transform offers great possibilities for such an analysis. In particular, here we adopt the adaptive harmonic wavelet transform (AHWT) proposed by Liu (2003) to analyze the baseline and test signals of Lamb wave propagation in the undamaged and test structures, respectively. With this as the basis for feature extraction, PCA and Hotelling's T^2 analysis are employed to highlight the feature, remove the noise effect and finally identify the response anomaly with a given confidence level.

To facilitate the following discussions, here we briefly review the experimental configuration outlined in part I. We consider an aluminum beam structure in two states: undamaged and damaged. The experimental set-up in figure 1 shows the damaged beam with a single piezoelectric actuator and single sensor. In the damaged beam, a surface notch is introduced. The piezoelectric actuator is connected with a waveform generator while the sensor is connected with a digital oscilloscope. Since excitation signals with narrow bandwidth are preferred to reduce the dispersion of the Lamb wave, we use sinusoidal waves under a Hann window as the transient excitation signal. It is expressed as

$$f(t) = \frac{1}{2} \sin(\omega_0 t) \left[1 - \cos\left(\frac{2\pi t}{T}\right) \right], \quad t < T \quad (1)$$

where ω_0 is the center frequency and T is the duration of the excitation signal which is typically a multiple of the half-period of the center frequency. Unless otherwise noted, in this paper T is selected as ten times the half-period. As introduced in part I, Lamb wave modes can be categorized as symmetric and antisymmetric based on the wave motions with respect to the median plane of the structure. In our case, we choose the center frequency lower than 160 kHz so that only the S_0 mode (the lowest symmetric mode) and the A_0 mode (the lowest antisymmetric mode) can be excited.

3.1. Adaptive harmonic wavelet transform for multi-signal applications

From the Fourier transform in the frequency domain

$$W_{mnk}(\omega) = \begin{cases} \frac{1}{(n-m)2\pi} e^{-i\omega \frac{k}{n-m}} & m2\pi \leq \omega \leq n2\pi \\ 0 & \text{otherwise.} \end{cases} \quad (2)$$

Newland (1993, 1994) derived the family of generalized harmonic wavelets

$$w_{mnk}(t) = w_{mn} \left(t - \frac{k}{n-m} \right) = \frac{\exp \left[i n 2 \pi \left(t - \frac{k}{n-m} \right) \right] - \exp \left[i m 2 \pi \left(t - \frac{k}{n-m} \right) \right]}{(n-m) i 2 \pi t} \quad (3)$$

where m and n are the level parameters, $0 \leq m < n$, and an integer k denotes the translation parameter within the level (m, n) . Notice that each level (m, n) corresponds to one wavelet function that covers the frequency range $(m2\pi, n2\pi)$. Harmonic wavelets are orthogonal so that a complete set of them could be called a wavelet basis. They are compact in the frequency domain, where each wavelet can be related to an ideal bandpass filter. The advantage is that the signal analysis is restricted to specific frequency bands with known physical meanings and these bands are represented by the corresponding wavelet levels.

Here we employ a discrete algorithm to obtain the coefficients by computing the inverse discrete Fourier transform (IDFT) of successive blocks (each corresponding to a (m, n) level) of the Fourier coefficients. For a given Lamb wave response signal $s(t)$ represented by the time series $s(r)$, $r = 0, 1, \dots, N-1$, the corresponding complex wavelet coefficients can be obtained by computing

$$a_{mnk} = \sum_{l=0}^{n-m-1} F(m+l) \exp \left(\frac{i 2 \pi k l}{n-m} \right), \quad k = 0, 1, \dots, n-m-1 \quad (4)$$

where $F(q)$, $q = 0, 1, \dots, N-1$ are the Fourier coefficients calculated by discrete Fourier transform (or FFT)

$$F(q) = \frac{1}{N} \sum_{r=0}^{N-1} s(r) \exp \left(-\frac{i 2 \pi r q}{N} \right). \quad (5)$$

Moreover, in the discrete transform, each continuous wavelet function has to be replaced by a corresponding circular

continuous function

$$w_{mnk}^{(c)}(r) = \frac{1}{(n-m)} \sum_{l=m}^{n-1} \exp \left(i 2 \pi l \left(\frac{r}{N} - \frac{k}{n-m} \right) \right). \quad (6)$$

Thus, the signal $s(r)$ defined on the unit time interval can be expanded as

$$s(r) = \sum_{m,n} \sum_{k=m}^{n-1} \left\{ a_{mnk} w_{mnk}^{(c)}(r) + \bar{a}_{mnk} \bar{w}_{mnk}^{(c)}(r) \right\}. \quad (7)$$

Each selection of level parameter pairs, e.g. $\{(m_0, n_0), (m_1, n_1), \dots, (m_{L-1}, n_{L-1})\}$, must begin with a pair for which $m_0 = 0$ and continue with touching (but not overlapping) pairs until $n_{L-1} = N_f$, where N_f corresponds to the Nyquist frequency and L denotes the number of levels (Newland 1993, 1994).

Liu (2003) treated each selection $\{(m_0, n_0), (m_1, n_1), \dots, (m_{L-1}, n_{L-1})\}$ as a partition of $\Omega = \{0, 1, \dots, N_f\}$ and adopted a Shannon entropy-based algorithm (Coifman and Wickerhauser 1992) to search a partition tree for the best partition (in the sense that the signal can be represented most sparsely). For any time series $\mathbf{x} = \{x_j\}$, the Shannon entropy is defined as

$$H(\mathbf{x}) = - \sum_j p_j \log p_j \quad (8)$$

where $p_j = |x_j|^2 / \|\mathbf{x}\|^2$ and $p_j \log p_j$ is set to be 0 if $p_j = 0$. The entropy shown above is a measure of the sparsity, and therefore we expect smaller entropy for a better partition. The iteration procedure for a sequence of 16 elements using a binary partition tree is illustrated in figure 2. Since $N_f = 9$ in this case, there are 9 Fourier coefficients left for the partition algorithm. For the initial partition, we consider each inverse Fourier coefficient as an initial subgroup, whose Shannon entropy is called the initial entropy. Here notice that each subgroup represents an aforementioned (m, n) pair corresponding to a wavelet. In the second partition, IDFT is applied to every two successive Fourier coefficients to form a subgroup, whose entropy is calculated and compared with the sum of the corresponding initial entropies. As in the example shown in figure 2, the sum entropy of the first two initial subgroups is smaller so that they are kept after the first selection. Through the entire iteration, the wavelet coefficients associated with the 'best' partition are computed. Meanwhile, the 'best' wavelet basis is generated by the same partition.

The advantages of the above-outlined adaptive harmonic wavelet transform (AHWT) over other wavelet transforms, like Daubechies 4, can be seen from the example illustrated in figure 3. Figure 3(a) shows an experimental signal used as the input of the transforms to be compared. The signal is the waveform collected by the piezoelectric sensor from the aforementioned damaged beam with the center frequency at 90 kHz. Based on the information of the frequency contents, we could identify noise-related contents on the AHWT map, i.e. in figure 3(b), the low frequency content around 0 kHz is due to the vibration of the experiment base, while the noise from the experimental equipment results in high frequency content at around 300 kHz. On the other hand, the content

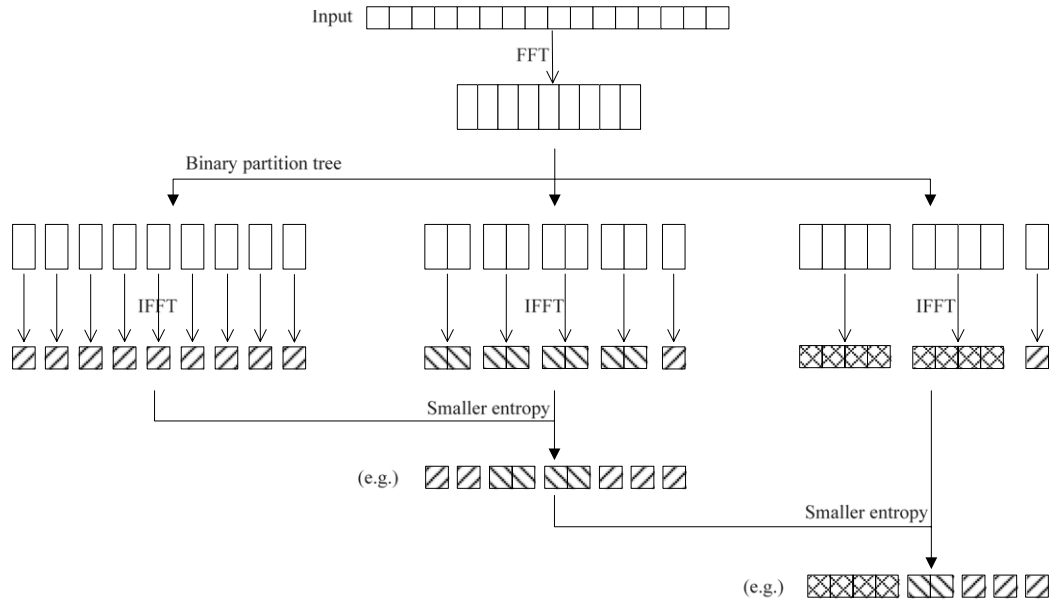


Figure 2. Discrete time adaptive harmonic wavelet transform implemented using FFT/IFFT ($N = 16$).

around 100 kHz, which is associated with the received Lamb waves, could be called signal-related content. In contrast to the signal-related content, which varies over time as the sensor signal does, the noise-related content remains unchanged over the entire time span. The excitation frequency of the actuation signal is set as 90 kHz; therefore, the features of the received signal have been highlighted and interpreted physically in the AHWT domain. In comparison, we cannot directly differentiate the features from the noise on the wavelet coefficient map shown in figure 3(c), where the discrete Daubechies 4 wavelet is used. From figure 3(d), we can see a similar pattern in the continuous Daubechies 4 wavelet domain but could not interpret it directly. This is because its wavelet scale is not directly associated with physical parameters. It is also worth mentioning that Daubechies 4 wavelet transforms, which cannot be implemented by FFT, are of lower computational efficiency than AHWT.

AHWT is signal-dependent, i.e. multiple signals measured from the same structure may lead to different ‘best’ wavelet bases, due to the environmental and operational variances. In order to build a consistent baseline dataset from multiple signals, our detection algorithm requires a common wavelet basis for all the signals to be compared. In other words, the problem becomes how to find a common wavelet basis such that the overall performance of the wavelet transforms from all the baseline signals could be maximized. It is worth mentioning that we have used the entropy to measure the performance of each wavelet transform, and entropies are addable for independent events. Thus, a natural idea is to use the summation of all the entropies as a measure of the overall performance. Recall that each time series $\mathbf{s}_l = \{s_l(r), r = 0, 1, \dots, N - 1\}$ ($l = 1, 2, \dots, L$ is the sequence number) collected from the piezoelectric sensors generates a ‘best’ wavelet basis $\{\mathbf{w}_{mnk}\}_l$ and an vector of

wavelet coefficients \mathbf{a}_l . An entropy $H(\mathbf{a}_l)$ can then be obtained for \mathbf{a}_l . Thus, if all L signals are projected on $\{\mathbf{w}_{mnk}\}_l$, then a matrix of wavelet coefficients $\mathbf{A}_l = [\mathbf{a}_1 \ \mathbf{a}_2 \ \dots \ \mathbf{a}_L]_l$ can be obtained. Here we define the total Shannon entropy for \mathbf{A}_l

$$H(\mathbf{A}_l) = H(\mathbf{a}_1) + H(\mathbf{a}_2) + \dots + H(\mathbf{a}_L) \quad (9)$$

where $l = 1, 2, \dots, L$. Since high sparsity is our objective in the basis selection, we select the common wavelet basis $\{\mathbf{w}_{mnk}\}_u$ such that the corresponding matrix of wavelet coefficients $\mathbf{A}_u = [\mathbf{a}_1 \ \mathbf{a}_2 \ \dots \ \mathbf{a}_L]_u$ have the smallest total Shannon entropy, i.e.

$$u = \arg \min_l H(\mathbf{A}_l). \quad (10)$$

The baseline dataset is then chosen as \mathbf{A}_u . By applying the same wavelet basis to the newly collected signal, we can obtain the new data vector to be compared with \mathbf{A}_u . This procedure ensures that the features extracted from the multiple baseline signals are comparable with the features extracted from the newly collected signals, while all the advantages of AHWT remain.

3.2. Feature highlighting and quantitative decision making

Principal component analysis (PCA) is a multivariate statistical procedure that transforms a number of correlated variables into a smaller number of uncorrelated new variables called the principal components (Jackson 1991). The first principal component accounts for as much of the variation in the data as possible, and each succeeding component explains as much of the remaining variability as possible. By eliminating the information not contained in the first few principal components, noise can then be reduced. PCA has been applied in a variety of applications including process monitoring and

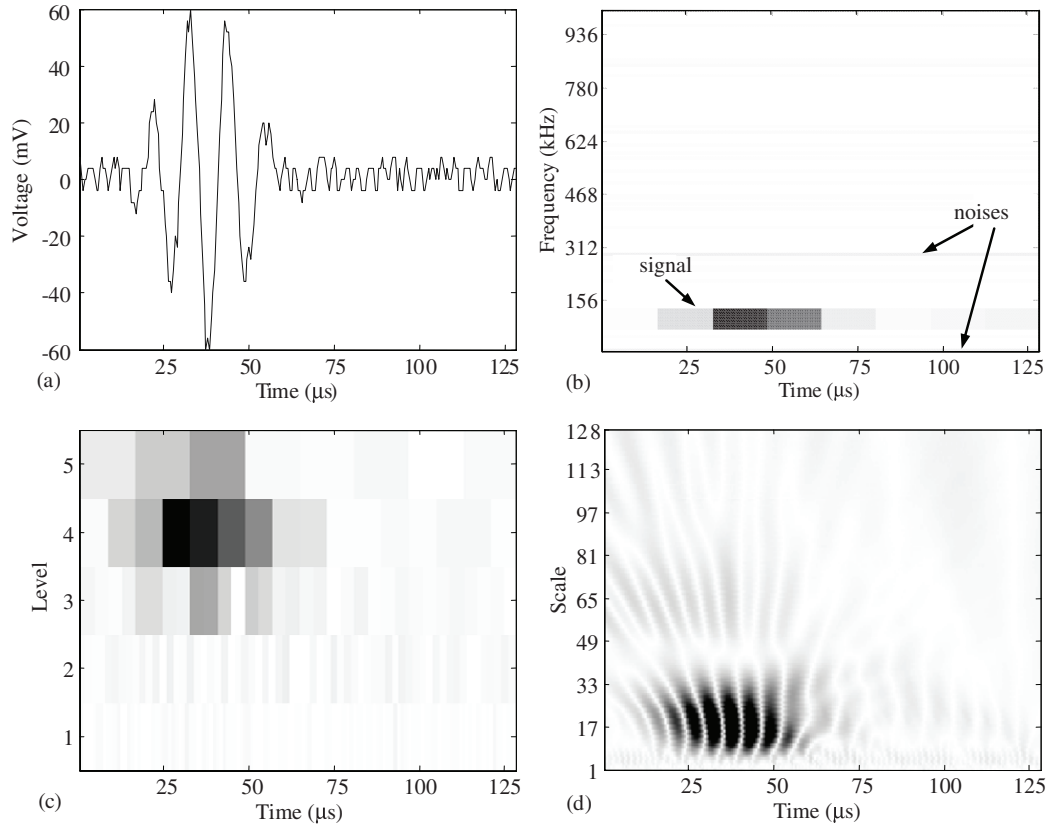


Figure 3. Comparing AHWt with Daubechies 4 wavelet transforms.

fault diagnosis (Dunia and Qin 1998, Akbaryan and Bishnoi 2001).

Consider a block of baseline data denoted by a $K \times L$ matrix \mathbf{X} , whose L column vectors $\mathbf{x}_1, \mathbf{x}_2, \dots, \mathbf{x}_L$ represent L signals, each with K coefficients (dimensions). Specifically in our application, the matrix \mathbf{X} is normally a part of the baseline dataset \mathbf{A}_u . We can obtain the covariance matrix $\mathbf{C} = \tilde{\mathbf{X}}\tilde{\mathbf{X}}^T / (L - 1)$ using $\tilde{\mathbf{X}} = [\mathbf{x}_1 - \boldsymbol{\mu} \quad \mathbf{x}_2 - \boldsymbol{\mu} \quad \dots \quad \mathbf{x}_L - \boldsymbol{\mu}]$, where vector $\boldsymbol{\mu}$ consists of the sample mean μ_k along each dimension ($k = 1, 2, \dots, K$). Note that the square root of the k th element along the main diagonal of the covariance matrix \mathbf{C} is the sample standard deviation σ_k along the k th dimension. By singular value decomposition, it yields an orthogonal (eigenvector) matrix $\mathbf{V} = [\mathbf{v}_1 \quad \mathbf{v}_2 \quad \dots \quad \mathbf{v}_K]$ and a diagonal (eigenvalue) matrix $\mathbf{D} = \text{diag}(\lambda_1, \lambda_2, \dots, \lambda_K)$ such that $\mathbf{CV} = \mathbf{VD}$. The eigenvalues are arranged in descending order $\lambda_j \geq \lambda_{j+1}$ for $j = 1, 2, \dots, K - 1$.

Theoretically, the denoising can be carried out by the following procedure. First we find the effective rank rk of \mathbf{X} such that $\lambda_{rk} \geq \varepsilon_1 > \lambda_{rk+1}$ (Konstantinides and Yao 1988), where ε_1 is the L_1 -norm of the noise. We then discard the eigenvectors (i.e. replacing them by zero) associated with $\lambda_{rk+1}, \dots, \lambda_K$ and form a modified eigenvector matrix \mathbf{V}_m . However, finding the optimal value of ε_1 without a specific noise model is generally difficult. Thus, in practice an alternative method is carried out to choose rk as the smallest number so that the accumulative energy is above a certain

threshold $ET\%$,

$$rk_0 = \min rk \quad \text{such that} \quad \sum_{j=1}^{rk_0} \lambda_j > ET\% \sum_{j=1}^K \lambda_j. \quad (11)$$

Here we recall that the eigenvalues represent the distribution of the original energy among each of the eigenvectors. The selection of an appropriate $ET\%$ will be discussed later in this paper.

Previous studies have shown that the orthogonal wavelet transform of fractal noise is Karhunen–Loève-like in terms of correlation structure (Wornel 1996), which means the signal-to-noise ratio (SNR) can be enhanced by concentrating signal information into a relatively smaller number of non-zero coefficients. Consider a data vector \mathbf{x}_t consisting of wavelet coefficients transformed from a test signal \mathbf{s}_t . First we need to standardize it using the same sample mean vector $\boldsymbol{\mu}$ and the sample standard deviation vector $\boldsymbol{\sigma}$ for the corresponding block of aforementioned baseline data blocks \mathbf{X} , $\mathbf{z} = (\mathbf{x} - \boldsymbol{\mu}) / \boldsymbol{\sigma}$. Then we obtain the reduced-space data $\mathbf{y} = \mathbf{V}_m^T \mathbf{z}$ by projecting \mathbf{z} onto \mathbf{V}_m . Finally the denoised data can be reconstructed as $\hat{\mathbf{x}} = \mathbf{V}_m \mathbf{y}$.

Now let us consider how to quantitatively indicate the potential damage from the obtained features. We adopt Hotelling's T^2 analysis, a widely used approach in multivariate analysis (MacGregor and Kourti 1995, Johnson and Wichern 2002). Its standard procedure consists of two phases. First, baseline data are subgrouped and used to establish an upper

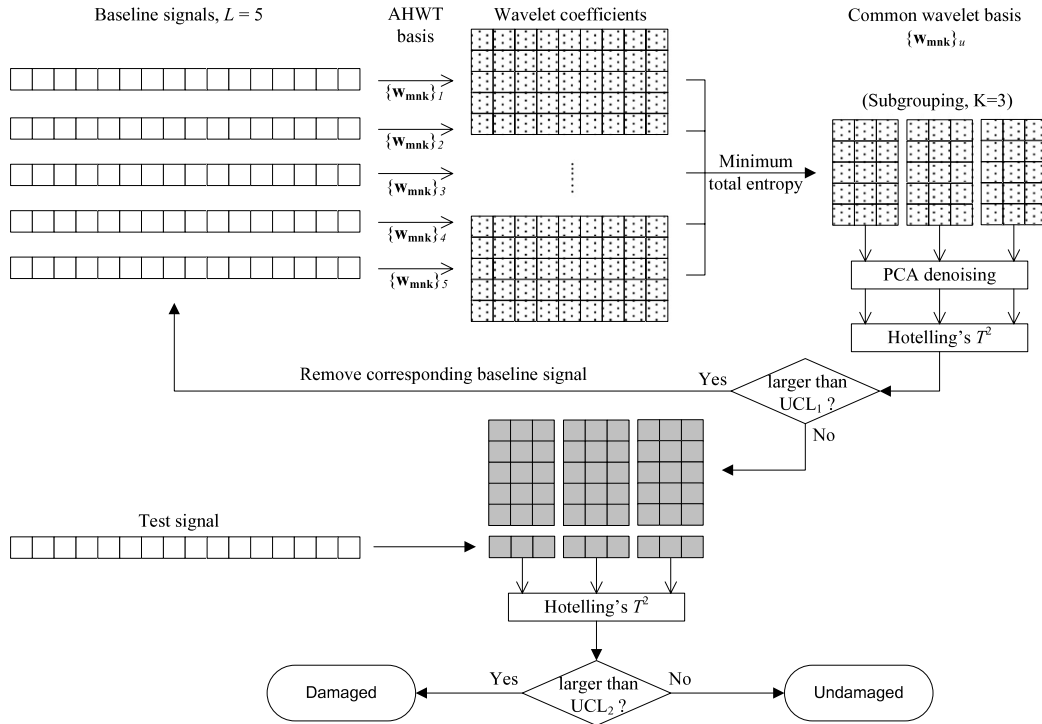


Figure 4. Procedure of the robust and quantitative decision making ($N = 16, L = 5, K = 3$).

control limit UCL_1 under a certain confidence level $100(1 - \alpha)\%$, where α indicates the error probability ($0 < \alpha < 1$). We consider a subgroup (block) of the denoised baseline dataset $\hat{\mathbf{X}} = [\hat{\mathbf{x}}_1 \dots \hat{\mathbf{x}}_L]$ with L signals, each having K points ($K < L$). Denote the signal mean vector and the covariance matrix as $\hat{\boldsymbol{\mu}}$ and $\hat{\mathbf{C}}$, respectively. The statistic T^2 for the l th signal $\hat{\mathbf{x}}_l$ is defined as $T_l^2 = (\hat{\mathbf{x}}_l - \hat{\boldsymbol{\mu}})\hat{\mathbf{C}}^{-1}(\hat{\mathbf{x}}_l - \hat{\boldsymbol{\mu}})^T, l = 1, 2, \dots, L$. It is known that Hotelling's T^2 follows the F distribution (Seber 1984), therefore the phase I upper control limit can be obtained as

$$UCL_1 = \frac{K(L-1)^2}{L(L-K)} F_\alpha(K, L-K) \quad (12)$$

with $F_\alpha(K, L-K)$ denoting the critical value for an F distribution with K and $L-K$ degrees of freedom. If any signal's T^2 value is beyond the upper control limit and assignable causes are determined, the corresponding signal is omitted from the baseline dataset. This procedure is called phase I self-checking. Following that, in phase II, a distinction is made between the baseline and the test data using a modified upper control limit UCL_2 . Assuming the test data is independent of the baseline data, the phase II upper control limit is modified as

$$UCL_2 = \frac{K(L-1)(L+1)}{L(L-K)} F_\alpha(K, L-K). \quad (13)$$

The processing of a test signal follows the same procedure as is done to the baseline dataset. If any calculated T^2 value exceeds the phase II upper control limit, we may conclude that, at the confidence level of $100(1 - \alpha)\%$, the analyzed structure is in a damaged state. This completes the development of the signal processing and decision-making methodology.

Figure 4 illustrates a complete procedure of detection decision making. First, five input signals from an undamaged structure are processed to build up the baseline dataset. Each input signal generates one 'best' wavelet basis and a corresponding matrix of wavelet coefficients using that basis. Here each matrix consists of $L = 5$ vectors, whose entropies are summed up as the total Shannon entropy of that matrix. We select the common wavelet basis as the one with the minimum total Shannon entropy, while the matrix is called the baseline dataset. PCA truncation is applied to the baseline dataset after subgrouping ($K = 3$), followed by Hotelling's T^2 analysis. The phase I upper control limit is used for the self-checking procedure, where outliers are eliminated and the baseline dataset is updated. After that, the test signal is processed using the identical common wavelet basis and then denoised by PCA truncation. Finally the T^2 chart quantitatively indicates the extent to which the test dataset in every subgroup deviates from the baseline. The damage detection decision is then made based on the statistical analysis at a certain confidence level.

4. Parametric analysis and case studies

In what follows we carry out detailed analysis and case studies of damage detection using the methodology outlined in the preceding section.

4.1. Detection demonstration

We start our discussion with a demonstration of our proposed methodology using experimental signals. We collect a group of eight time series from the undamaged beam and transform them to a matrix of wavelet coefficients using the procedure

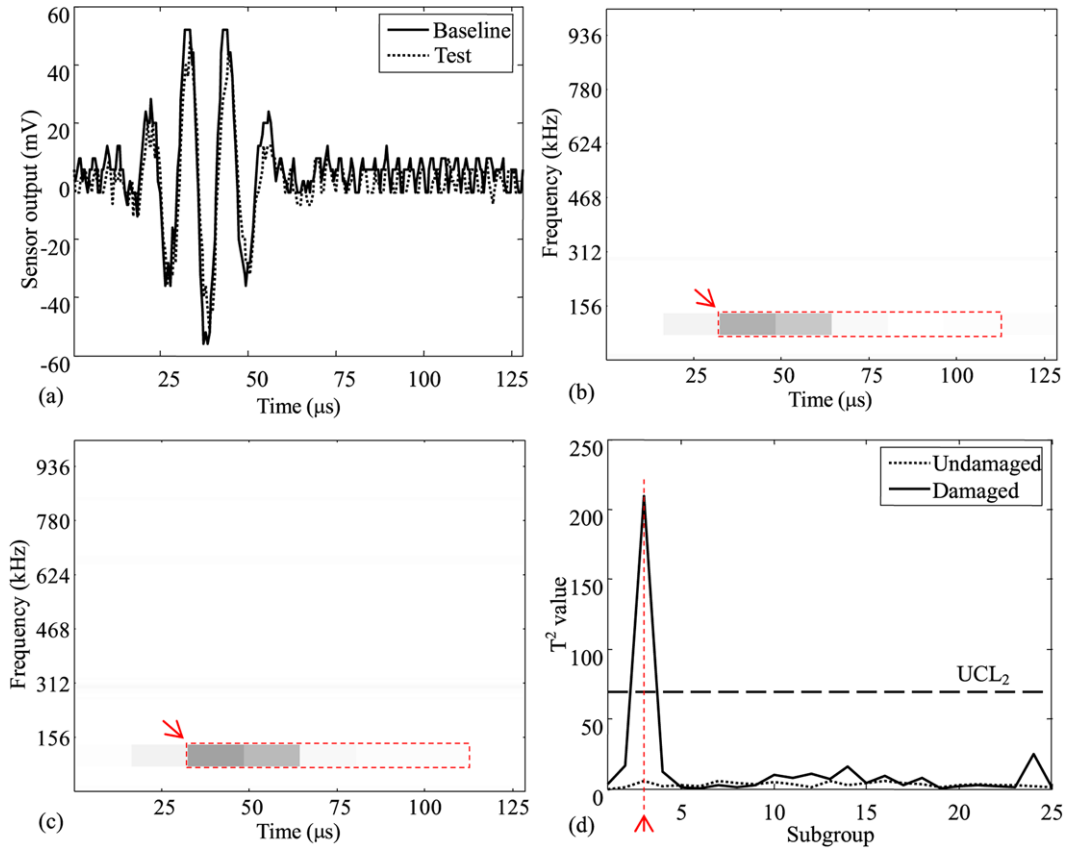


Figure 5. Damage detection demonstration. (Notch width $w = 0.8$ mm and depth $h/2d = 33.3\%$.)

developed in section 3. Figure 5(a) shows one baseline signal collected via experiment, together with one test signal collected on a test beam with a notch (width $w = 0.8$ mm and depth-to-beam-thickness ratio $h/2d = 33.3\%$). Notice that we need all the eight baseline signals for the following data processing, but the solid line in figure 5(a) represents only one of them. By applying the entropy based method described in section 3.1, the group of the baseline signals yields a common wavelet basis set. The baseline dataset is then obtained by projecting those baseline signals onto the common wavelet basis set. We subgroup the baseline dataset into several blocks to perform the PCA-based denoising, where μ and σ of each block are recorded for later use. Here we need to consider that small groups lead to more computation loops while large groups may average the deviation within a group and result in meaningless T^2 values. In addition, the subgroup size affects both degrees of freedom for the F distribution as used in equations (11) and (12). Therefore, adjusting the size is a complicated trade-off between computational efficiency and detection sensitivity. In this research, after comprehensive simulation studies we make each subgroup contain 5 wavelet coefficients. Next, outliers are eliminated from the baseline dataset through the phase I self-checking in Hotelling's T^2 analysis. Figure 5(b) exhibits the AHWT coefficient map for the baseline signal in figure 5(a), and figure 5(c) is the map for the test signal.

The test signal is then processed using the same wavelet basis and other relevant parameters such as μ and σ . After

that, the denoised test data vector is compared with the baseline dataset. A T^2 chart is plotted as the detection result, where each T^2 value indicates the deviation of the test data block from the corresponding baseline data block. If any T^2 value exceeds the phase II upper control limit, we may make a decision that the structure is damaged. Although it seems difficult to recognize the difference between the two wavelet maps by direct observation, the damage can be detected with 90% confidence from the T^2 chart, as shown in figure 5(d). We can see that the phase II upper control limit is around 70, while the critical subgroup, marked with an arrow in figure 5(d), is around 200. In the presence of noise, although the T^2 values may fluctuate case by case, we can always recognize the same critical subgroup via the T^2 chart. The AHWT coefficients belonging to the critical subgroup are also marked with arrows in figures 5(b) and (c). We can see that the marked block is around the center frequency of the excitation signal (i.e. 90 kHz in this case). In other words, we have verified that the frequency shift is insignificant as the Lamb waves travel through the notch, which has been numerically studied by Alleyne and Cawley (1992). We also randomly choose one baseline signal as the test signal to simulate the case of an undamaged test beam. The T^2 values are indicated by the dotted line in figure 5(d). Clearly, all of these values are well under the phase II upper control limit. In conclusion, the proposed robust and quantitative method can lead to correct decisions about the beam status, even in the presence of noise and other variations.

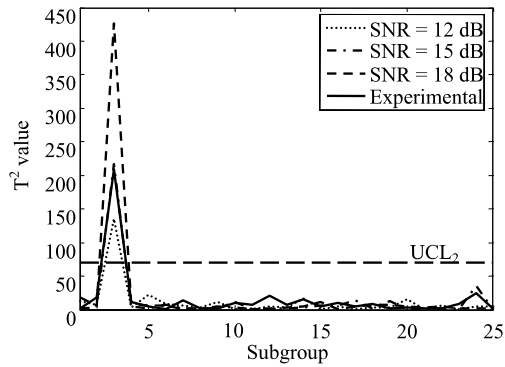


Figure 6. Detection sensitivity versus signal-to-noise ratio. (Notch width $w = 0.8$ mm and depth $h/2d = 33.3\%$.)

4.2. Estimation of additive noise for numerical simulations

In what follows we discuss the influence of parameters including the center frequency of the excitation signal and notch (damage) size. For such parametric analysis, we mainly use numerical simulation results from the direct finite element analysis. As introduced in part I, an undamaged beam structure is modeled in ANSYS and meshed mainly by SOLID45 elements with eight nodes and three degrees of freedom (DOF) per node. The Lamb waves are excited by applying pin forces to the nodes located at the two ends of the actuator. The sensor output is obtained through the summation of the strains along the center line of the sensor. The rectangular notch (i.e. the damage, with the same size as in section 4.1) is introduced by removing elements from the undamaged beam model. Finer meshes around the notch are employed.

In order to perform a parametric study with the finite element model, we incorporate noise into the simulation results so that a group of multiple baseline signals can be constructed numerically. We first estimate the level of the additive noise so that the noisy simulation signals can result in equivalent detection sensitivity compared with experimental signals. According to the central limit theorem, the artificial noise added to numerical signals is assumed as additive white Gaussian noise (AWGN). Figure 6 shows the detection results when using numerical signals with AWGN of different noise levels (SNR = 12, 15, 18 dB). Apparently, this AWGN blurs the numerical signals and therefore reduces the detection sensitivity. Here we regard the level of the noise added to the numerical signals as appropriate if its effect can represent the total effect of all the environmental variations and uncertainties associated with the experiments. In other words, the T^2 values calculated using the experimental signals should be the same as that using simulation outputs added with appropriate AWGN. By comparing the curves corresponding to different noise levels in figure 6, we can see that the numerical signals with SNR = 15 dB result in similar T^2 values as that using experimental signals. Clearly, SNR = 15 dB is a good estimate about the total noise effect. In the following analyses we construct multiple baseline signals as well as the test signal by adding AWGN onto the simulation results while keeping SNR = 15 dB.

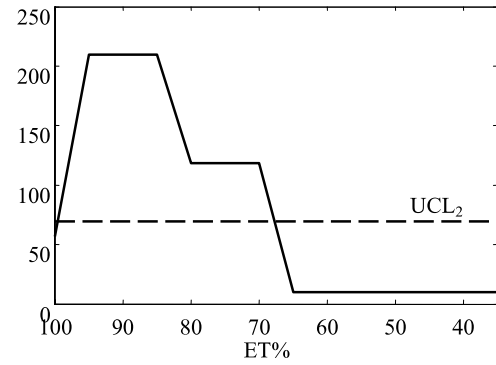


Figure 7. Detection sensitivity versus truncation threshold. (Notch width $w = 0.8$ mm and depth $h/2d = 33.3\%$.)

4.3. Truncation threshold $ET\%$ in PCA-based denoising

The truncation threshold $ET\%$, as introduced in equation (11), decides how many principal components are kept in the PCA-based denoising. If too many principal components are kept, meaning too little energy is regarded as noise, then the detection sensitivity would decrease due to the remaining noise. On the other hand, if too few principal components are kept, meaning some signal energy is removed, then the detection sensitivity would also decrease due to less information provided by the signal. Therefore, $ET\%$ is an important parameter influencing the effect of denoising. In our discussion, we consider the peak T^2 value which corresponds to the aforementioned critical subgroup as a measure of the detection sensitivity for each specific configuration. To study the truncation threshold $ET\%$, we use the same set of baseline and test signals as in section 4.1. Figure 7 shows the peak T^2 value versus $ET\%$ when other parameters remain the same. At first, all the principal components are kept when $ET\% = 100\%$ (no denoising). We can see that the peak T^2 value is below the phase II upper control limit, meaning no damage is detected. As $ET\%$ decreases to 90%, the peak T^2 value reaches its maximum which is above the control limit, meaning that the damage can be detected by the proposed method. When $ET\%$ goes below 90%, the peak T^2 value decreases again and finally stays below the control limit. Obviously, larger T^2 values would be preferred when processing the same signals, because the detection would be not only more sensitive to small damage but also more robust against signal noises. We thus choose $ET\% = 90\%$ for the following discussions so that T^2 values can be maximized for our specific case.

4.4. Detection sensitivity with respect to excitation frequency

Recall that the single piezoelectric actuator excites multiple Lamb modes simultaneously, which in our specific case are the S_0 mode and the A_0 mode. As suggested by Giurgiutiu (2003, 2005), damage detection should be carried out at the center frequency where the peak wave amplitude ratio between the S_0 mode and the A_0 mode is the maximum. That center frequency is referred to as the 'sweet spot'. This 'sweet spot' frequency has been analyzed systematically in part I

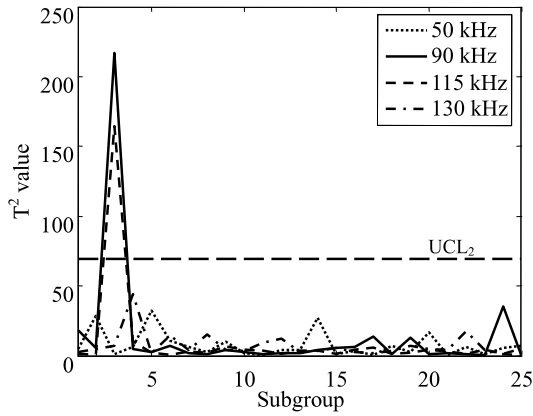


Figure 8. Detection sensitivity versus center frequencies of the excitation signal. (Notch width $w = 0.8$ mm and depth $h/2d = 33.3\%$.)

and verified through analytical, numerical and experimental analyses. For our specific case, the ‘sweet spot’ excitation frequency is 90 kHz. Figure 8 shows the T^2 values calculated using numerical signals with AWGN for different center frequencies. As demonstrated in section 4.1, here we add AWGN to the numerical simulation so that a group of eight baseline signals can be obtained with SNR = 15 dB. The test signal is then obtained in the same manner. We note that the ‘sweet spot’ 90 kHz indeed leads to better detection sensitivity than other frequencies.

Since the ‘sweet spot’ depends on both the S_0 and A_0 Lamb modes, we want to evaluate the individual effects of the S_0 and A_0 Lamb modes under the proposed robust decision-making methodology. Since pure S_0 or A_0 mode excitation cannot be achieved by a single actuator, in this particular discussion we use two actuators attached on the top and bottom surfaces of the structure. Thus, pure symmetric Lamb wave modes can be excited by applying in-phase excitation signals onto both actuators, while antisymmetric modes can be excited by applying out-of-phase excitation signals. Correspondingly, we modify our numerical simulation

by introducing the equivalent set-ups shown in figure 9, where the set-up for generating mixed S_0 and A_0 modes in figure 9(a) can be replaced by those in figures 9(b) and (c). The actuators in figure 9(b) generate a pure S_0 mode while those in figure 9(c) generate a pure A_0 mode. The summation equality holds for the signals received by the piezoelectric sensor. Examples of the corresponding time domain signals are shown in figures 9(d)–(f), respectively. Figure 10 shows the detection results for the cases where a pure S_0 mode or a pure A_0 mode is excited. Each subplot corresponds to one excitation frequency: 50, 90, 115 or 130 kHz.

In part I of this two-paper series, we have discussed, through a case study, from the mechanistic standpoint, the effects of S_0 and A_0 Lamb modes on the damage detection. In that analysis which does not involve noise, we defined an energy index to quantify the difference between wave patterns from undamaged and damaged structures. As the excitation frequency rises from 50 to 130 kHz, the energy difference increases and then decreases with the maximum reached at 90 kHz (Wang *et al* 2007). Here we can quantify the difference between signals (under noise) using the methodology developed in this paper. As shown in figure 8, the same trend can be observed for the peak T^2 values, where both the baseline and test signals are contaminated by artificial noises. The discussion in part I also showed that the pure S_0 mode leads to a similar trend, while the pure A_0 mode leads to an opposite trend (i.e. negative energy difference). These can now be verified by the peak T^2 values in figure 10, where the pure S_0 mode always leads to better detection results than the pure A_0 mode. In particular, the peak T^2 value is about 350 for the case that the 90 kHz pure S_0 mode is excited (figure 10(b)), while that for the case of the pure A_0 mode is only around 50 (below the control limit). In comparison, the mixed modes lead to a peak T^2 value of about 220 (figure 8). This indicates that the detection sensitivity is negatively affected by the excited A_0 mode. Using the quantitative decision-making method, we have thus verified that for our specific case the ‘sweet spot’ frequency (around 90 kHz) leads to the optimal detection sensitivity, in the presence of noises.

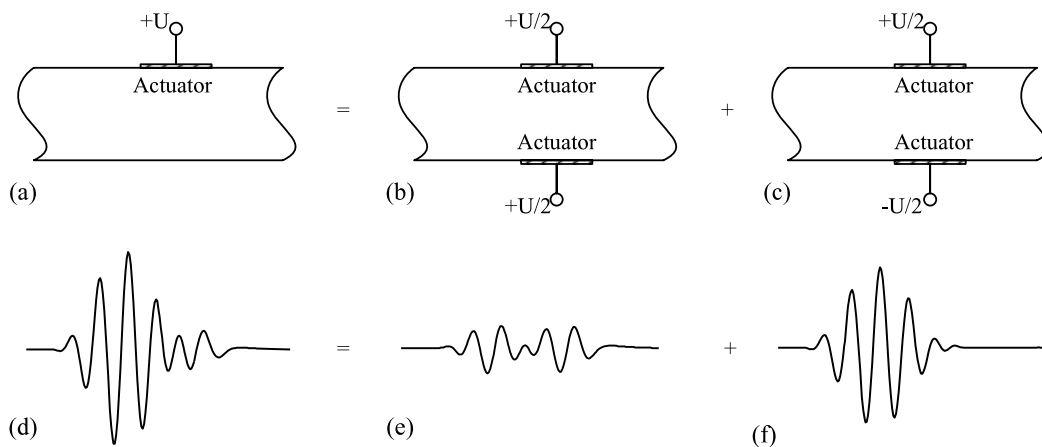


Figure 9. Equivalent set-ups for generating (a) mixed modes, (b) pure S_0 mode and (c) pure A_0 mode Lamb waves. The same equity holds for the sensor signals (d)–(f).

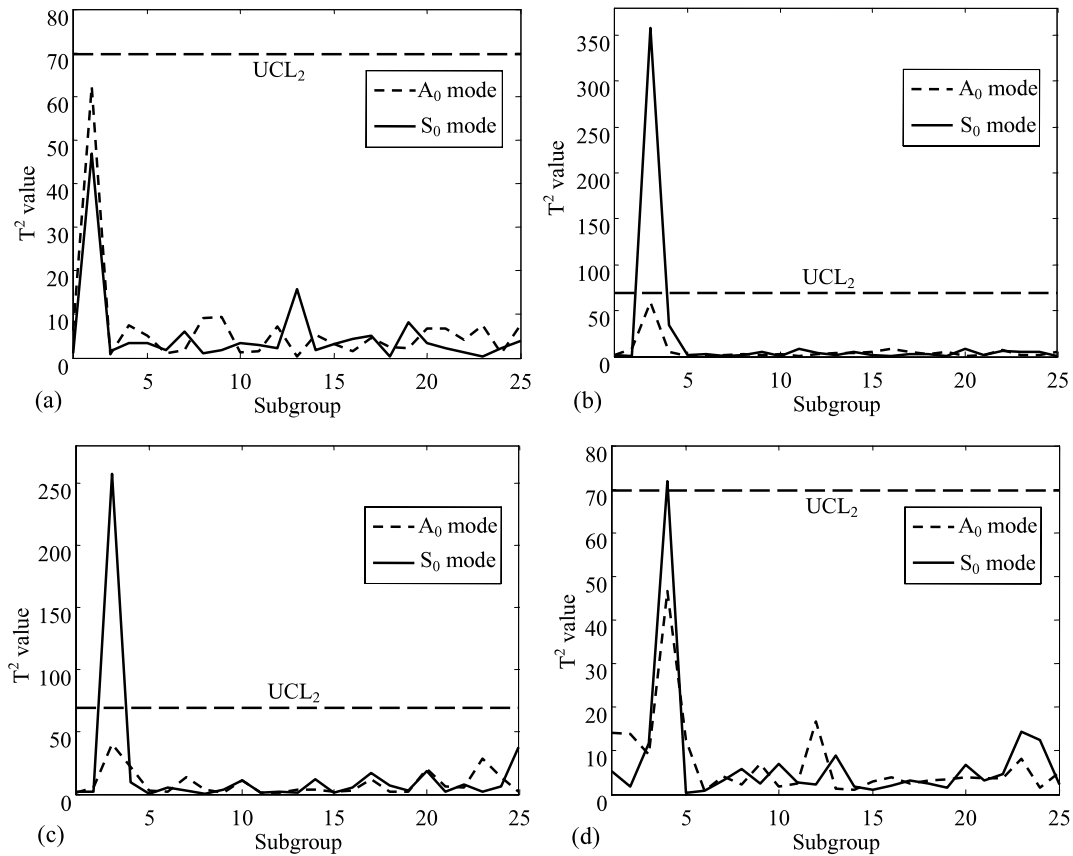


Figure 10. Detection using pure A_0 or pure S_0 mode Lamb waves excited at (a) 50 kHz, (b) 90 kHz, (c) 115 kHz and (d) 130 kHz. (Notch width $w = 0.8$ mm and depth $h/2d = 33.3\%$.)

4.5. Detection sensitivity versus notch depth and width

After analyzing the parameters of the experiment and simulation, we now discuss the detection sensitivity versus the notch depth/width. It is worth mentioning that the single actuator set-up (figure 9(a)) is used for the following discussion to simulate the effect of mixed S_0 and A_0 modes. In general, larger notches cause more wave energy reflection than smaller notches do, which means more significant difference would be observed in sensor signals. Therefore, we may expect a higher T^2 value for larger notches. In our case, the notch size is determined by two parameters: depth and width.

We first vary the notch depth and keep the notch width fixed at 0.8 mm. By modifying the finite element model, we can numerically obtain sensor outputs for different notch depths (from 16.7% to 44.4%). Figure 11(a) shows the detection results as a function of $h/2d$. We can see that T^2 values increase as the notch depth increases, meaning that the deeper notches greatly weaken the transmitted wave energy. For the confidence level $100(1 - \alpha)\% = 90\%$, it can be seen from figure 11(a) that a 0.8 mm wide notch with $h/2d = 22.2\%$ can be successfully detected.

In comparison, figure 11(b) shows the detection results for notches with different width when we keep the notch depth fixed as $h/2d = 33.3\%$. We can see that the T^2 value does not change too much as the notch width changes,

meaning that the notch width is not a major factor in the detection sensitivity. Similar observations have been discussed by Alleyne and Cawley (1992) in terms of transmission and reflection ratios. From figures 11(a) and (b), we confirm that, when the notch width is small compared to the wavelength, as is usually the case in practice, the major factor in the detection sensitivity is the notch depth.

5. Concluding remarks

In this research, we developed a combination of signal processing tools for the analysis of Lamb-wave-based damage detection using piezoelectric transducers. An improved adaptive harmonic wavelet transform approach was used to extract the common features from multiple baseline signals. This was followed by principal component analysis for feature highlighting and denoising. Quantitative decision making was realized by using Hotelling T^2 analysis that declares damage occurrence under given confidence level. Collectively, these analysis tools lead to a robust and quantitative damage detection methodology. Experimental, numerical and analytical studies were carried out on a laboratory beam structure to demonstrate and verify the detection performance. A series of parametric studies were performed. The results validated the mechanistic analysis developed in part I of

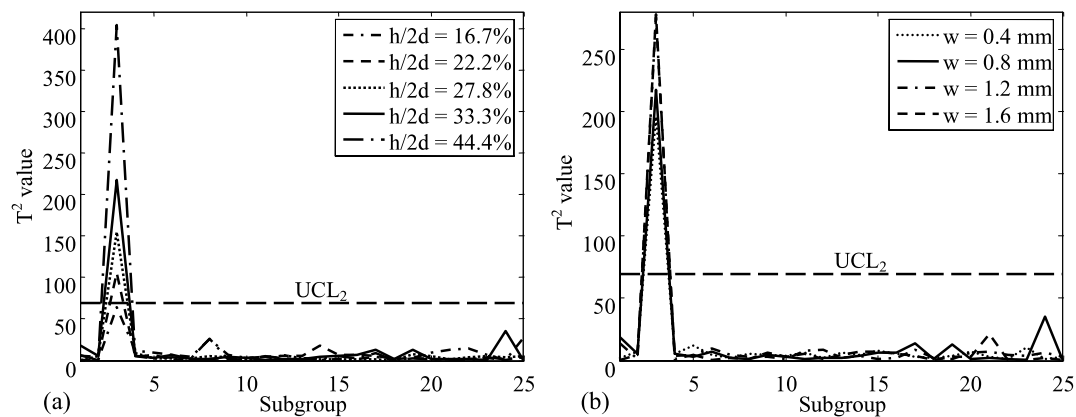


Figure 11. Detection sensitivity versus (a) notch depth (when $w = 0.8$ mm is fixed) and (b) notch width (when $h/2d = 33.3\%$ is fixed).

this two-paper series from the statistical and data analysis standpoint, and also provided general guidelines for damage detection implementation.

Acknowledgments

This research is supported by the National Science Foundation under grants CMMI 0428210 and CMMI 0427878.

References

- Akbaryan F and Bishnoi P R 2001 Fault diagnosis of multivariate systems using pattern recognition and multisensor data analysis technique *Comput. Chem. Eng.* **25** 1313–39
- Alleyne D N and Cawley P 1992 The interaction of Lamb waves with defects *IEEE Trans. Ultrason. Ferroelectr. Freq. Control* **39** 381–97
- Cawley P and Adams R D 1979 The location of defects in structures from measurements of natural frequencies *J. Strain Anal. Eng. Des.* **14** 49–57
- Coifman R R and Wickerhauser M V 1992 Entropy-based algorithms for best basis selection *IEEE Trans. Inf. Theory* **38** 713–8
- Doebbling S W, Farrar C R, Pnme M B and Shevitz D W 1996 Damage identification and health monitoring of structural and mechanical systems from changes in their vibration characteristics: a literature review *Los Alamos National Laboratory Report LA-13070-MS*
- Dunia R and Qin S J 1998 Joint diagnosis of process and sensor faults using principal component analysis *Control Eng. Practice* **6** 457–69
- Fang X and Tang J 2006 Damage detection of engine bladed-disks using multivariate statistical analysis *Proc. SPIE Smart Struct. Mater.* **6174** 707–14
- Ganesan R, Das T K and Venkataraman V 2004 Wavelet-based multiscale statistical process monitoring: a literature review *IIE Trans.* **36** 787–806
- Giurgiutiu V 2003 Lamb wave generation with piezoelectric wafer active sensors for structural health monitoring *Proc. SPIE Smart Struct. Mater.* **5056** 111–22
- Giurgiutiu V 2005 Tuned Lamb wave excitation and detection with piezoelectric wafer active sensors for structural health monitoring *J. Intell. Mater. Systems Struct.* **16** 291–306
- Giurgiutiu V, Bao J and Zhao W 2003 Piezoelectric wafer active sensor embedded ultrasonics in beams and plates *Exp. Mech.* **43** 428–49
- Hou Z, Noori M and Amand R S 2000 Wavelet-based approach for structural damage detection *J. Eng. Mech.* **126** 677–83
- Jackson J E 1991 *A User's Guide to Principal Components* (New York: Wiley)
- Johnson R A and Wichern D W 2002 *Applied Multivariate Statistical Analysis* 5th edn (Englewood Cliffs, NJ: Prentice-Hall)
- Kessler S S and Dunn C T 2003 Optimization of Lamb wave actuating and sensing materials for health monitoring of composite structures *Proc. SPIE Smart Struct. Mater.* **5056** 123–33
- Kim H and Melhem H 2004 Damage detection of structures by wavelet analysis *Eng. Struct.* **26** 347–62
- Konstantinides K and Yao K 1988 Statistical analysis of effective singular value in matrix rank determination *IEEE Trans. Acoust. Speech Signal Process.* **36** 757–63
- Lin X and Yuan F G 2001a Diagnostic Lamb waves in an integrated piezoelectric sensor/actuator plate: analytical and experimental studies *Smart Mater. Struct.* **10** 907–13
- Lin X and Yuan F G 2001b Detection of multiple damages by prestack reverse-time migration *AIAA J.* **39** 2206–15
- Liu B 2003 Adaptive harmonic wavelet transform with applications in vibration analysis *J. Sound Vib.* **262** 45–64
- Lu C J and Hsu Y T 1999 Vibration analysis of an inhomogeneous string for damage detection by wavelet transform *Int. J. Mech. Sci.* **44** 745–54
- MacGregor J F and Kourti T 1995 Statistical process control of multivariate processes *Control Eng. Practice* **3** 403–14
- Newland D E 1993 Harmonic wavelet analysis *Proc. Math. Phys. Sci.* **443** 203–25
- Newland D E 1994 Harmonic and musical wavelets *Proc. Math. Phys. Sci.* **444** 605–20
- Niethammer M 1999 Application of time frequency representations to characterize ultrasonic signals *MS Thesis* Georgia Institute of Technology, Atlanta
- Okimoto G and Lemonds D 1999 Principal component analysis in the wavelet domain: new features for underwater object recognition *Proc. SPIE* **3710** 697–708
- Papoulis A 1962 *The Fourier Integral and its Applications* (New York: McGraw-Hill) pp 63–7
- Park S, Yun C-B, Roh Y and Lee J-J 2006 PZT-based active damage detection techniques for steel bridge components *Smart Mater. Struct.* **15** 957–66
- Peng Z K and Chu F L 2004 Application of the wavelet transform in machine condition monitoring and fault diagnostics: a review with bibliography *Mech. Syst. Signal Process.* **18** 199–221
- Quek S T, Wang Q, Zhang L and Ong K H 2001 Practical issues in the detection of damage in beams using wavelets *Smart Mater. Struct.* **10** 1009–17
- Raghavan A and Cesnik C E S 2005 Finite-dimensional piezoelectric transducer modeling for guided wave based structural health monitoring *Smart Mater. Struct.* **14** 1448–61

- Seber G A F 1984 *Multivariate Observations* (New York: Wiley)
- Staszewski W J 2002 Intelligent signal processing for damage detection in composite materials *Compos. Sci. Technol.* **62** 941–50
- Tseng K K-H and Naidu A S K 2002 Non-parametric damage detection and characterization using smart piezoceramic material *Smart Mater. Struct.* **11** 317–29
- Tua P S, Quek S T and Wang Q 2004 Detection of cracks in plates using piezo-actuated Lamb waves *Smart Mater. Struct.* **13** 643–60
- Wang Q, Wang D and Su X 1999 Crack detection of structure for plane problem with spatial wavelets *Acta Mech. Sin.* **15** 39–51
- Wang X, Lu Y and Tang J 2007 Damage detection using piezoelectric transducers and the Lamb wave approach: I system analysis *Smart Mater. Struct.* **17** 025033
- Wornel G 1996 *Signal Processing with Fractals: A Wavelet Based Approach* (Englewood Cliffs, NJ: Prentice-Hall)
- Yan G, Zhou L L and Yuan F G 2005 Wavelet-based built-in damage detection and identification for composites *Proc. SPIE Smart Struct. Mater.* **5765** 324–34
- Yu L and Giurgiutiu V 2005 Advanced signal processing for enhanced damaged detection with piezoelectric wafer active sensors *Smart Struct. Systems* **1** 185–215
- Yu L and Giurgiutiu V 2006 Damage detection using guided waves and piezoelectric wafer active sensor arrays *Proc. IMAC XXIV (St Louis, MO, Jan.–Feb. 2006)* p 170
- Zhao B, Yang P, Basir O A and Mittal G S 2006 Ultrasound based glass fragments detection in glass containers filled with beverages using neural networks and short time Fourier transform *Food Res. Int.* **39** 686–95